This is a preprint, the final version is subject to change, of the American Mineralogist (MSA)
Cite as Authors (Year) Title. American Mineralogist, in press.
(DOI will not work until issue is live.) DOI: http://dx.doi.org/10.2138/am-2016-5558

Revision 3

Effects of differential stress on the structure and Raman spectra of calcite from first-principles calculations

Liu Lei[a,*], Lv Chaojia[a], Zhuang Chunqiang[b], Yi Li[a], Liu Hong[a], Du Jianguo[a]

[a] Key Laboratory of Earthquake Prediction, Institute of Earthquake Science, China Earthquake Administration, No.63 Fuxing Road, Haidian District, Beijing, China.

[b] Institute of Microstructure and Properties of Advanced Materials, Beijing University of Technology, 100 Pingleyuan, Chaoyang District, Beijing, 100124, China

Abstract: Differential stresses are expected to influence the properties of minerals. The structural and Raman vibrational properties of calcite under hydrostatic and differential stresses were studied using a first-principles method based on density functional theory. Our results show that the density of calcite increases or decreases under different differential stress, relative to its value under hydrostatic pressure. The calculated effects of differential stress on bond lengths are nominal. As pressure increases, the frequencies of all Raman modes increase, with their pressure derivatives slightly depending on the differential stress. The state of stress influences the Raman modes by shifting their frequencies to either higher or lower values relative to the corresponding hydrostatic results. In particular, the largest and smallest frequency shifts were predicted for E_g-156 and A_{1g}-1086 modes, respectively, when the additional stress was applied along the *a*-axis. Visualization of atomic motions associated with Raman modes suggests that the differential stress-induced shifts in Raman frequencies are controlled by out-of-plane vibrations of atoms. The stress estimated on the basis of the experimentally measured shift of the Raman frequency of calcite sample gathered from the Wuchuan earthquake fault by applying our calculated dv_i/dP value of A_{1g}-1085 mode is 785 MPa, which appears to be comparable to the stress inferred at the Wuchuan earthquake focus. Thus, the first-principles simulations and Raman

spectroscopy experiments together may help us in elucidating the state of stress in the Earth's interior.

Keywords: Differential stress, Structure, Raman vibrational properties, Calcite, First-principles

Introduction

Differential stress exists in the Earth's interior. It can be produced by tectonic compression or by deep fluid movement, particularly at plate boundaries or minerals' grain boundaries thereby possibly driving plate tectonics and causing earthquakes. The effects of differential stress on the properties of minerals are shown or expected to be substantial (Demouchy et al. 2011; Sato et al. 2013; Liu et al. 2014). Therefore, the state of differential stress in the Earth's interior, particularly its distribution in space and its time-dependent evolution, is a fundamental issue in geoscience. However, this issue has yet to be fully understood (Solberg et al. 1978; Kidder 2012).

Calcite is one of the most abundant minerals in the Earth's continental crust. Understanding its structural, spectral, and mechanical properties under differential stress is important for understanding the mechanical behavior of rock and the state of stress in the deep Earth. The X-ray diffractive and Raman spectral detection have been widely used to determine the crystal structure and Raman spectrum of minerals. In particular, laser Raman spectroscopic analysis of minerals (such as quartz) allows us to investigate the pressure conditions in metamorphic rocks (Enami et al. 2007). As an important rock-forming mineral, calcite is usually abundant in fault and tectonic boundaries. So, if we quantify how the crystal structure and Raman frequencies of calcite behave under different stress conditions, we can infer the state of stress of fault or tectonic boundaries by measuring the structure and/or Raman spectrum of calcite gathered from the sites. Several investigations of the stress state of the Earth's interior have been reported (Enami et al. 2007), by focusing on the relationship between

pressure and Raman frequency shift of minerals (Liu and Mernagh 1990; Dean et al. 1982; Prencipe et al. 2004; Schmidt and Ziemann 2000). In general, these investigations have been performed under hydrostatic pressure.

However, determining the complex microstructures of multiple mineral phases in mineral assemblages and rocks under non-hydrostatic stress or differential stress represents a formidable challenge. For example, the questions of what non-hydrostatic stresses can be developed and how much of the differential stress state can be preserved remain unanswered (Weathers et al. 1979; Christie and Ord 1980; Demouchy et al. 2011; Angel et al. 2014). At present, quantitatively investigating the effects of differential stress on the structure and Raman spectrum is difficult by experiments. Alternatively, the first-principles methods can be used to accurately calculate various properties of minerals at the atomic scale (Gillan et al. 2006 ; Jahn and Kowalski 2014), including the state of differential stress and its effects (Parrinello and Rahman 1982; Liu et al. 2014). Here, we investigated the structure and Raman spectra of calcite from first-principles calculations to quantify the effects of differential stress on these properties.

Computational method

Crystal structure of calcite

Calcite is a carbonate mineral with trigonal symmetry (space group: $R\ \bar{3}c$, two formula units (Z) per cell). The structure consists of layers of Ca ions alternating with stacks of carbonate layers along the c axis of the hexagonal cell. The carbonate layers are composed of planar triangular shaped carbonate ions (CO_3^{2-}), with a carbon atom at the center of the triangle and the three oxygen atoms at each corner (Fig. 1). The irreducible representation of the optical vibrations of calcite for D3 factor

group (Fateley et al. 1972) is described by:

$$\Gamma_{op}=A_{1g}+3A_{2g}+4E_g+2A_{1u}+4A_{2u}+6E_u,$$

where $A_{1g}+4E_g$ represents Raman-active, $1A_{2u}+4E_u$ infrared active, $1A_{2u}+1E_u$ acoustic, and $3A_{2g}+2A_{1u}$ spectroscopically inactive (silent) modes.

First-principles computational details

The first-principles calculations were performed using density functional perturbation theory (Refson et al. 2006), density functional theory (Hohenberg and Kohn 1964; Kohn and Sham 1965), and plane wave pseudopotential method, as implemented in the CASTEP codes (Clark et al. 2005). Local density approximation (Ceperley and Alder 1980; Perdew and Zunger 1981) was used for describing exchange-correlation interaction. Norm conserving pseudopotentials (Hamann et al. 1979) were used to model electron-ion interaction, with plane wave cutoff of 900 eV. A 4×4×1 Monkhorst Pack grid of k points was adopted for sampling Brillouin zone. A convergence criterion of 5×10-7a.u. on the total energy was used in the self-consistent field calculations.

The structure and Raman spectroscopy of calcite at given pressures were calculated by simultaneously optimizing both atomic positions and lattice constants under Hellmann–Feynman forces and stresses acting on nuclei and lattice parameters, respectively (Nielsen and Martin 1983). Spatial derivatives of the macroscopic polarization were calculated numerically along eigenvectors of each Raman active phonon mode according to the polarization for each displacement using linear response formalism (Gonze 1997). Once these derivatives are determined, the Raman cross-section through appropriate averaging space can be calculated. Further details can be found in Porezag and Pederson (1996) and Refson et al (2006). The calculated results on the structural, elastic, and vibrational

properties of calcite are in good agreement with previous results (Supplementary Table 1.), thus demonstrating the validity of our calculations.

The setting and expression of the differential stress

Different stresses were applied to the crystal along *a-, b-,* and *c*-axis directions (i.e., *x*, *y*, and *z* directions) marked as σ_{xx}, σ_{yy}, and σ_{zz} (Fig. 1). Thus, the equivalent hydrostatic pressure (***P***, GPa) applied to crystals is $(\sigma_{xx} + \sigma_{yy} + \sigma_{zz})/3$. When $\sigma_{xx} = \sigma_{yy} = \sigma_{zz}$, the pressure is hydrostatic; when $\sigma_{xx} \neq \sigma_{yy} \neq \sigma_{zz}$, the pressure is differential stress. Therefore, if σ_{xx} is equal to $\boldsymbol{P_1}$, σ_{yy} is equal to $\boldsymbol{P_1}$, and σ_{zz} is equal to $\boldsymbol{P_1} + \boldsymbol{x}$ GPa, then ***P*** is equal to $\boldsymbol{P_1} + \boldsymbol{x/3}$ GPa, differential stress is $\boldsymbol{\Delta}\sigma_{xx} = \sigma_{xx} - \boldsymbol{P} = -\boldsymbol{x}/3$ GPa, $\boldsymbol{\Delta}\sigma_{yy} = \sigma_{yy} - \boldsymbol{P} = -\boldsymbol{x}/3$ GPa, and $\boldsymbol{\Delta}\sigma_{zz} = \sigma_{zz} - \boldsymbol{P} = 2\boldsymbol{x}/3$ GPa. The largest stress difference among σ_{zz}, σ_{yy}, and σ_{xx} is ***x*** GPa. Totally, five sets of different crystal structure and Raman spectrum of calcite were calculated under differential stresses and hydrostatic pressure.

Results and discussion

Effects of stress on cell parameters

Figure 2 shows the calculated lattice parameters of calcite as a function of pressure. The *a*- and *c*-axes decrease by 0.63 and 5.09% from 0 to 5 GPa. The ***c***-axis is thus much more compressible than the ***a***-axis, thus implying highly anisotropic compression of calcite.

The lattice constant ***a*** increases and ***c*** decreases under differential stresses of $\Delta\sigma_{xx}:\Delta\sigma_{yy}:\Delta\sigma_{zz} = -1/6:-1/6:2/6$ and $= -1/3:-1/3:2/3$ relative to their equivalent hydrostatic values (Fig.2). The differences of *a*- and *c-axis* from their equivalent hydrostatic values when $\Delta\sigma_{xx}:\Delta\sigma_{yy}:\Delta\sigma_{zz} = -1/6:1/3:-1/6$ and $= -1/3:2/3:-1/3$ are opposite to those when $\Delta\sigma_{xx}:\Delta\sigma_{yy}:\Delta\sigma_{zz} = -1/6:-1/6:2/6$ and =

−1/3:−1/3:2/3. The lattice constants are smaller (larger) than their hydrostatic counterparts when the positive (negative) differential stresses are applied along the axis direction. The effect on lattice constant increases linearly with increasing differential stress.

As shown in Fig.2, the density increases by 0.23% (0.0067 g/cm^3) and 0.46% (0.0134 g/cm^3) $\Delta\sigma_{xx}$:$\Delta\sigma_{yy}$:$\Delta\sigma_{zz}$ of −1/6:−1/6:1/3 and = −1/3:−1/3:2/3, respectively, with respective to its hydrostatic value. On the other hand, the density decreases by 0.13% (0.0037 g/cm^3) and 0.20% (0.0058 g/cm^3) when $\Delta\sigma_{xx}$:$\Delta\sigma_{yy}$:$\Delta\sigma_{zz}$ = −1/6:1/3:−1/6 and = −1/3:2/3:−1/3, respectively. The magnitude of these density shifts also increases with increasing differential stress. The differential stress-induced changes in the density of calcite are larger than those previously predicted for forsterite (0.003 g/cm^3 for under the differential stress of $\Delta\sigma_{xx}$:$\Delta\sigma_{yy}$:$\Delta\sigma_{zz}$ = −1/3:2/3:−1/3 (Liu et al. 2014).

When pressure increases from 0 to 5 GPa, the calculated C–O and Ca–O bond lengths decrease by 0.34, and 1.84%, respectively, and the calculated Ca–O octahedral volume decreases by 5.33% (Supplementary Fig.1). Compared to its value under hydrostatic pressure, the octahedral volume slightly increases when $\Delta\sigma_{xx}$:$\Delta\sigma_{yy}$:$\Delta\sigma_{zz}$ = −1/6:−1/6:2/6 and = −1/3:−1/3:2/3 and decreases when $\Delta\sigma_{xx}$:$\Delta\sigma_{yy}$:$\Delta\sigma_{zz}$ = −1/6:1/3:-1/6 and = −1/3:2/3:-1/3 (Fig.3). However, the effects of differential stress on the bond lengths are negligible.

Vibrational pattern of Raman modes

The calcite structure can be viewed in terms of independent Ca^{2+}-ion and carbonate-ion (CO_3^{2-}) units. The Raman modes of calcite given by $\Gamma_{op} = A_{1g} + 4E_g$ can be grouped into three categories: translation (*T*), rotation (*R*), and internal libration (*I*). The four E_g modes show all vibrational types (*T*, *R*, and *I*) but the A_{1g} mode shows only *I*-type vibration (Bhagavantam and Venkatarayudu 1969). We

identified the vibrational pattern of each calcite Raman mode by visualizing the associated atomic motions (vibrational direction and intensity of atoms) with the aid of animation of the computed vibrational modes built into the CASTEP package. These vibrational patterns are illustrated in Fig. 4.

The atomic vibrations associated with the E_g-156 mode include out-of-plane translations of two O atoms of planar carbonate unit and in-plane vibrations of one O and one C atom parallel to the ***b***-axis, that is, (001) crystal face. The relative vibrational intensities (i.e., the magnitudes of displacements) of the four atoms of the carbonate unit do not differ substantially. The E_g-284 mode includes out-of-plane translations of O and C atoms, and the vibrational intensity of the O atom is greater than that of the C atom. In the case of the E_g-712 mode, its vibrations mainly correspond to the nearly in-plane rotation of two O atoms and in-plane libration of one O and one C atom parallel to the *b*-axis. Similar to the E_g-156 mode, the vibrational intensity of the four atoms of a carbonate do not substantially differ. The vibrational properties of the E_g-1434 mode are similar to those of the E_g-156 mode, involving out-of-plane translations of two O atoms and in-plane libration of one O and one C atom with different vibrational directions. However, in this case, the vibrational intensity of the O atom is much smaller than that of the C atom. The vibration of the A_{1g}-1086 mode corresponds only to the stretching of C–O bonds. The C atom remains stable, whereas the O atoms move. The Ca^{2+} ions are not involved in any of the five Raman vibrational modes.

Effects of hydrostatic stress on the Raman frequency

The directions and intensities of the vibrations of all the atoms involved in the Raman modes remain nearly unchanged with increasing pressure. Though pressure does not affect the vibrational modes significantly, its effects on vibrational frequencies are substantial. The pressure derivatives

($d\nu_i/dP$) of five Raman frequencies under hydrostatic pressure are listed in Table 1. All Raman frequencies systematically increase with increasing pressure. Among the E_g vibrational modes, E_g-284 has the largest pressure derivative and E_g-712 has the smallest derivative. Our calculated pressure derivatives of the E_g and A_{1g} modes compare favorably with previous experimental and calculated results (Liu and Mernagh 1990; Gillet et al. 1993).

According to the anisotropic compression of calcite, pressure likely affects the out-of-plane vibrations more strongly than the in-plane vibrations of Raman modes. Therefore, the E_g-284 mode exhibits stronger pressure dependence. In the cases of the E_g-156 and E_g-712 modes, the O atoms and C atoms have similar relative vibrational intensities and these modes exhibit relatively small pressure derivatives. In the case of E_g-284 and E_g-1434, the relative vibrational intensities of the O atoms and C atoms differ, resulting in relatively high values of frequency-pressure derivatives. Thus, the difference between the relative vibrational intensities of the O atoms and C atoms can explain partly the differences in the pressure derivatives of Raman frequencies. As the difference between the relative vibrational intensities of O atoms and C atoms increases, Raman frequency depends more strongly on pressure.

Raman modes under differential stress

The vibrational directions and intensities of atoms under differential stresses show patterns similar to those under hydrostatic pressure (Fig. 5). Also, the pressure derivatives of all modes under differential stresses are similar to those under hydrostatic pressure; the differences being less than 0.3 cm^{-1}/GPa. Some new Raman peaks appeared under differential stress but their intensities are small. For the characteristic Raman modes of calcite, the frequencies change under differential stresses. Relative

to the values under hydrostatic pressure, the Eg-156 mode frequency shifts to higher value by 2.6 cm^{-1} under $\Delta\sigma_{xx}:\Delta\sigma_{yy}:\Delta\sigma_{zz} = -1/6:-1/6:1/3$, but to lower value by 1.1 cm^{-1} under $\Delta\sigma_{xx}:\Delta\sigma_{yy}:\Delta\sigma_{zz} = -1/6:1/3:-1/6$ (Table 2). The E_g-284 and E_g-1434 modes show the similar shift pattern except their smaller values under differential stresses. For all three modes, the two differential stress states show opposite (positive and negative) shifts on Raman frequency. However, the E_g-712 mode shows negative shifts of 0.7 and 0.9 cm^{-1} under both the differential stress states ($\Delta\sigma_{xx}:\Delta\sigma_{yy}:\Delta\sigma_{zz} = -1/6:-1/6:1/3$ and $-1/6:1/3:-1/6$). Finally, the differential stresses induce little or no frequency shifts in the case of the A_{1g}-1086 mode. Our results thus show that the differential stress has the strongest and weakest effects on the frequency shifts in the cases of the E_g-156 and A_{1g}-1086 mode, respectively. For all modes except A_{1g}-1086, the magnitude of the frequency shift increases with the increasing differential stress.

When the additional stress was applied along the *c*-axis, the differential stress affects the in-plane vibrations of atoms much less than the out-of-plane vibrations (the plane refers to (001) crystal face). As discussed above, the atomic vibrations associated with the E_g-156 and E_g-284 modes include some out-of-plane vibration, but the atomic vibrations associated with E_g-712, E_g-1434, and A_{1g}-1086 modes mostly include the in-plane vibration. The differential stress does not affect the in-plane bond distance (C-O bond) much (Fig.3), therefore, the E_g-156 and E_g-284 modes show larger frequency shifts than the E_g-712, E_g-1434, and A_{1g}-1086 modes.

When the additional stress was applied along the *c*-axis, the *c*-axis becomes smaller than its equivalent hydrostatic pressure value and the intensities of out-of-plane vibration of atoms increase thereby shifting the E_g-156 and E_g-284 modes to higher frequency. On the other hand, when the additional stress was applied along the *a*-axis, *c*-axis is larger than its equivalent hydrostatic pressure value and the intensities of out-of-plane vibration of atoms decrease thereby shifting these modes to

lower frequency. This means that the differential stress-induced frequency shifts are mainly controlled by the out-of-plane vibrations of atoms. For E_g-712, the frequency shifts to lower value for the cases of additional stress.

Conclusions and implication

Our first-principles results on the structural and Raman vibrational properties of calcite under pressure and differential stresses may help advance our knowledge about the state of stress or gravity in the earth's interior. First, we summarize our main findings: The effects of differential stress are to increase or decrease the lattice constants and the density of calcite depending on the stress type. The calculated pressure derivatives of all Raman modes of calcite under differential stresses are positive and similar to those under hydrostatic pressure. Our results show that the Raman vibrational frequencies are sensitive to differential stress, with E_g-156 and A_{1g}-1086 modes showing the largest and smallest shifts, respectively. The state of stress also affects the Raman frequencies, shifting to either higher or lower value, that is, showing positive or negative shifts with respect to the corresponding hydrostatic values. Therefore, the relationship between pressure and the Raman frequencies of minerals investigated using hydrostatic pressure (Asell and Nicol 1968; Schmidt and Ziemann 2000; Liu and Mernagh 1990; Gillet et al. 1993) is not valid under non-hydrostatic stress conditions. To investigate state of stress in metamorphic rocks (Enami et al. 2007), laser Raman spectroscopic analysis can relate Raman frequencies shifts with changes of differential stress.

Here, we show what the calculated effects of differential stress (and pressure) on Raman frequency shifts can tell us about the state of stress of minerals. The stress determined by the core differential strain analysis method in the Wenchuan-Earthquake Fault Scientific Drilling (WFSD)

project located at Hongkou town, Dujiangyan city, Sichuan province shows that in situ stress in the Earth's interior increases with increasing depth and ranges from 69.1 MPa (maximum principle stress) to 35.3 MPa (minimum principle stress) at a depth of 1.19 km (Peng et al. 2011). These measurements also demonstrate that differential stress exists in the Earth's interior. We extrapolated the results to the 19-km focal depth of the Wenchuan earthquake (magnitude 7.9, Eastern Sichuan, China; USGS; May 12, 2008) and obtained the maximum and minimum principle stresses of 1110 MPa and 566 MPa, respectively. The Raman peaks associated with A_{1g}-1085 mode of calcite collected from the Wenchuan earthquake fault (Shenxigou fault at Hongkou town, Dujiangyan city, Sichuan province) were observed to be shifted 2.7 cm^{-1} toward higher frequencies (Xie et al. 2015). Then the residual stress in calcite crystal is 785MPa on the base of our calculated dv_i/dP value of $A_{1g\text{-}1085}$ mode. The value is close to the stress at 19km depth in WFSD thereby suggesting that stress of seismic fault is similar to the stress of hypocenter. Unfortunately, the effects of differential stress on A_{1g}-1085 mode are too small for deducing and verifying the state of differential stress. If we know the shifts of other Raman modes such as their E_g-156 and E_g-712 modes for the sample, the state of differential stress can be deduced. We anticipate that this approach can be applied to other several mineral samples gathered at the same sites (the fault or other tectonic zone), such as quartz, feldspar, etc. so that we can obtain more specific information about the state of stress. Our study thus demonstrates that we can learn about the state of stress in the Earth's interior by combining first-principles simulations and Raman spectroscopy studies.

Acknowledgements

This work was supported by Key Laboratory of Earthquake Prediction, Institute of Earthquake Science, CEA (2012IES010201) and the National Natural Science Fund, China (41174071 and 41373060).

References

Angel, R.J., Matteo, A., Mattia, M., Paolo, N., and Fabrizio, N. (2014) How much differential stress can a rock support? 2014EGUGA.16.2086A.

Asell, J. F., and Nicol, M. (1968) Raman spectrum of α-quartz at high pressure. The Journal of Chemical Physics, 49, 5395-5399.

Bhagavantam, S., and Venkatarayudu, T. (1969) Theory of groups and its application to physical problems. Academic Press, New York.

Ceperley, D.M., and Alder, B.J. (1980) Ground state of the electron gas by a stochastic method. Physical Review Letters, 45, 566-569.

Christie, N. J., and Ord, J. M. A. (1980) Flow stress from microstructures of mylonites: example and current assessment. Journal of Geophysical Research, 85, 6253–6262,

Clark, S. J., Segall, M. D., Pickard, C. J., Hasnip, P. J., Probert, M. J., Refson, K., and Payne, M. C. (2005) First principlemethods using CASTEP. Zeitschrift für Kristallographie 220, 567-570.

De La Pierre, M., Carteret, C., Maschio, L., André, E., Orlando, R., and Roberto., D. (2014) The Raman spectrum of $CaCO_3$ polymorphs calcite and aragonite: A combined experimental and computational study. The Journal of Chemical Physics, 140, 164509-1-12.

Dean, K. J., Sherman, W. F., and Wilkinson, G. R. (1982) Temperature and pressure dependence of the Raman active modes of vibration of α-quartz. Spectrochimica Acta, 38A, 1105-1108.

Demouchy, S., Mainprice, D., Tommasi, A., Couvy, H., Barou, F., Frost, D.J., and Cordier, P. (2011) Forsterite to wadsleyite phase transformation under shear stress and consequences for the Earth's mantle transition zone. Physics of the Earth and Planetary Interiors, 184, 91–104.

Enami, M., Nishiyama, T., and Mouri, T. (2007) Laser Raman microspectrometry of metamorphic quartz: A simple method for comparison of metamorphic pressures. American Mineralogy, 92, 1303-1315.

Fateley, W.G., Dollish, F.R., Mcdevitt, N.T., and Bentley F.F. (1972) Infrared and Raman Selection Rules for Molecular and Lattice ibrations: The Correlation Method, Wiley-Interscience, New York.

Gillan, M. J., Alfe, D., Brodholt, J., Vocadlo, L., and Price, G.D. (2006) First-principles modeling of Earth and planetary materials at high pressures and temperatures. Reports on Progress in

Physics, 69, 2365-2441.

Gillet, P., Biellmann, C., Reynard, B., and McMillan, P. (1993) Raman spectroscopic studies of carbonates Part I: high-pressure and high-temperature behavior of calcite, magnesite, dolomite and aragonite. Physics and Chemistry of Minerals, 20, 1-18.

Gonze, X. (1997) First-principles responses of solids to atomic displacements and homogeneous electric fields: Implementation of a conjugate-gradient algorithm. Physical Review B, 55, 10337-10354.

Hamann, D. R., Schluter, M., and Chiang, C. (1979) Norm-Conserving Pseudopotentials. Physical Review Letters, 43, 1494-1497.

Hohenberg, P., and Kohn, W. (1964) Inhomogeneous electron gas. Physical Review B., 136, 864-871.

Jahn, S., and Kowalski, P. (2014) Theoretical approaches to structure and spectroscopy of earth materials. Reviews in Mineralogy and Geochemistry, 78(1), 691-743.

Kidder, S. B. (2012) Microstructural, metamorphic and experimental constrains on differential stress and temperature in the middle crust. Doctor Thesis, California Institute of Technology, Pasadena, California, USA.

Kohn, W., and Sham, L. J. (1965) Self-consistent equations including exchange and correlation effects. Physical Review A, 140, 1133-1138.

Liu, L., Du, J., Liu, H., and Yi, L. (2014) Differential stress effect on structural and elastic properties of forsterite by first principles simulation. Physics of the Earth and Planetary Interiors, 233, 95-102.

Liu, L.G., and Mernagh, T.P. (1990) Phase transitions and Raman spectra of calcite at high pressures and room temperature. American Mineralogist, 75, 801-806,

Nielsen, O.H., and Martin, R.M. (1983) First-principles calculation of stress. Physical Review Letters, 50, 697-700.

Parrinello, M., and Rahman, A. (1982) Strain fluctuations and elastic constants. The Journal of Chemical Physics, 76, 2662.

Peng, H., Ma, X., and Jiang, J. (2011) In-situ stress measurement by differential strain analysis method in WFSD-1. Journal of Geomechanics, 17(3), 249-261.

Perdew, J.P., and Zunger, A. (1981) Self-interaction correction to density functional

approximations for many-electron systems. Physical Review B, 23, 5048-5079.

Porezag, D., and Pederson M. R. (1996) Infrared intensities and Raman-scattering activities within density-functional theory. Physical Review B, 54, 7830.

Refson, K., Tulip, P.R., and Clark, S.J. (2006) Variational density-functional perturbation theory for dielectrics and lattice dynamics. Physical Review B, 73, 155114.

Sato, T., Funamori, N., and Yagi, T. (2013) Differential strain and residual anisotropy in silica glass. Journal of Applied Physics, 114, 103509.

Schmidt, C., and Ziemann, M.A. (2000) In-situ Raman spectroscopy of quartz: A pressure sensor for hydrothermal diamond-anvil cell experiments at elevated temperatures. American Mineralogy, 85, 1725-1734.

Solberg, P. H., Lockner, D. A., Summers, R. S., Weeks, J. D., and Byerlee, J. D. (1978) Experimental fault creep under constant differential Stress and high confining pressure. American Rock Mechanics Association ARMA-78-0146.

Weathers, M. S., Bird, J. M., Cooper, F. R., and Kohlstedt, D.L. (1979) Differential stress determined from deformation-induced microstructures of the Moine thrust zone. Journal of Geophysical Research, 84, 7495–7509.

Xie, C., Zhou, B., and Liu, L. (2015) Characteristics of Raman spectra of minerals in the veins of Wenchuan earthquake fault zone. Spectroscopy and Spectral Analysis, 35(1), 118-121 (in chinese).

Tables

Table 1 Pressure shifts of the Raman modes

Symmetry	E_g-156	E_g-284	E_g-712	E_g-1434	A_{1g}-1086	Reference
ν_{i0} (cm^{-1})	164.6	297.3	696.0	1441.2	1086.9	This study
	156	281	711	1434	1085	Liu and Mernagh 1990
$d\nu_i/dP$ (cm^{-1}/GPa)	3.2	5.7	1.9	4.9	3.4	This study
	2.5	5.3	2.2	5.9	9	Liu and Mernagh 1990
	2.3	6	1.7	3	7.5	Gillet et al. 1993

Table 2 Shifts of Raman frequencies under differential stress with respective to its hydrostatic value

	Symmetry					State of stress
	E_g-156	E_g-284	E_g-712	E_g-1434	A_{1g}-1086	$\Delta\sigma_{xx} : \Delta\sigma_{yy} : \Delta\sigma_{zz}$
Shift of frequency (cm^{-1})	2.6	1.2	-0.7	0.6		-1/6 : -1/6 : 1/6
	5.3	2.5	-1.1	0.9		-1/3 : -1/3 : 2/3
	-1.1	-1.3	-0.9	-0.1		-1/6 : 1/3 : -1/6
	-2.7	-2.3	-2.3	-0.3		-1/3 : 2/3 : -1/3

Notes: The positive values mean shift toward higher frequency, and negative values mean shift toward lower frequency

Figures

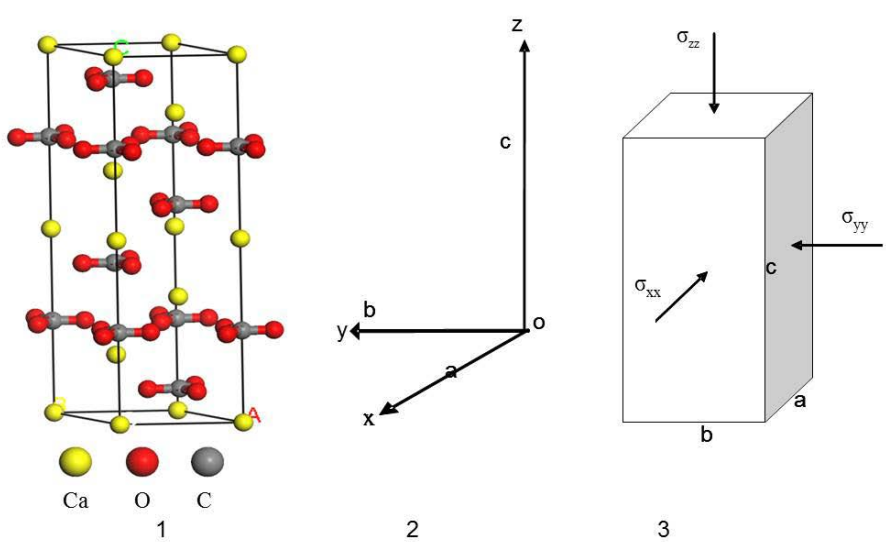

Fig. 1. Atomic structure of calcite and schematic diagram of differential stress project. (1) Atomic

structure, (2) Lattice constants and directions, and (3) Applied stresses (σ_{xx}, σ_{yy}, and σ_{zz}).

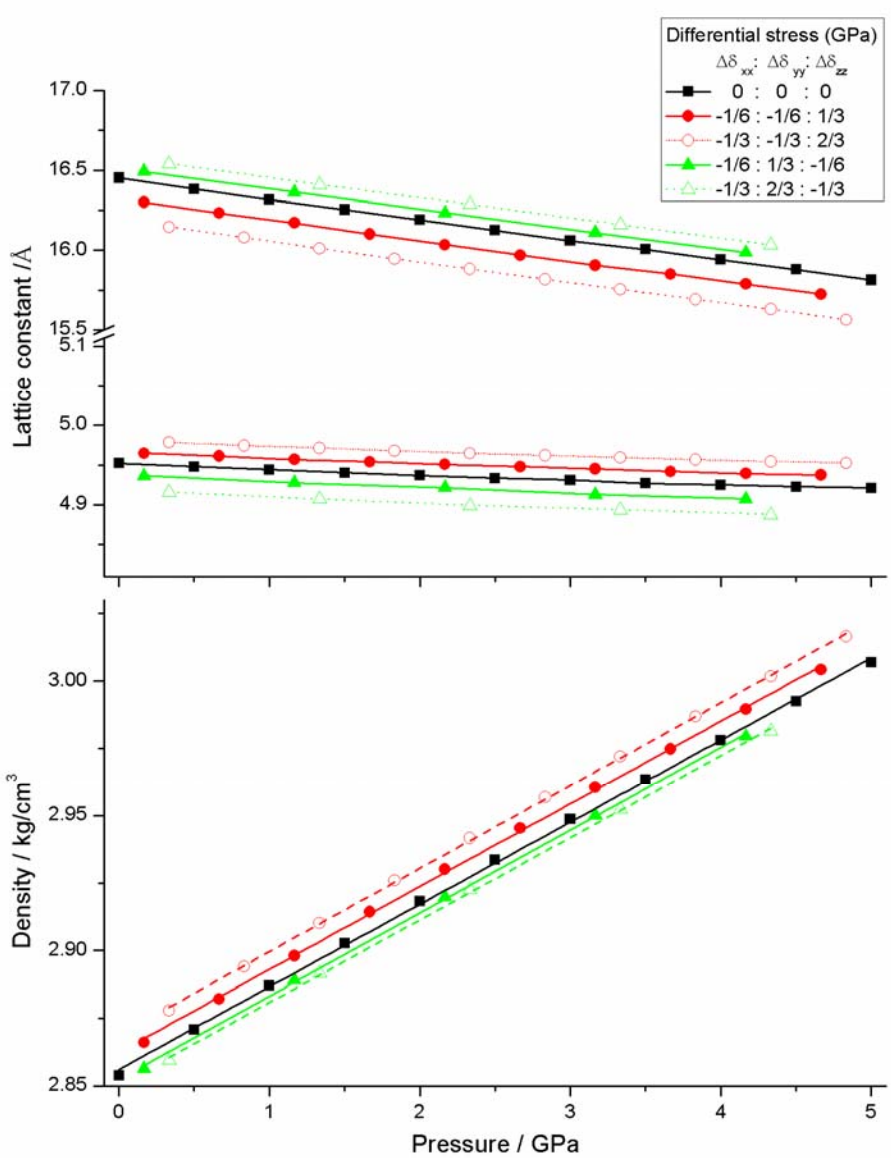

Fig. 2 Changes of lattice constants and density of calcite with pressure

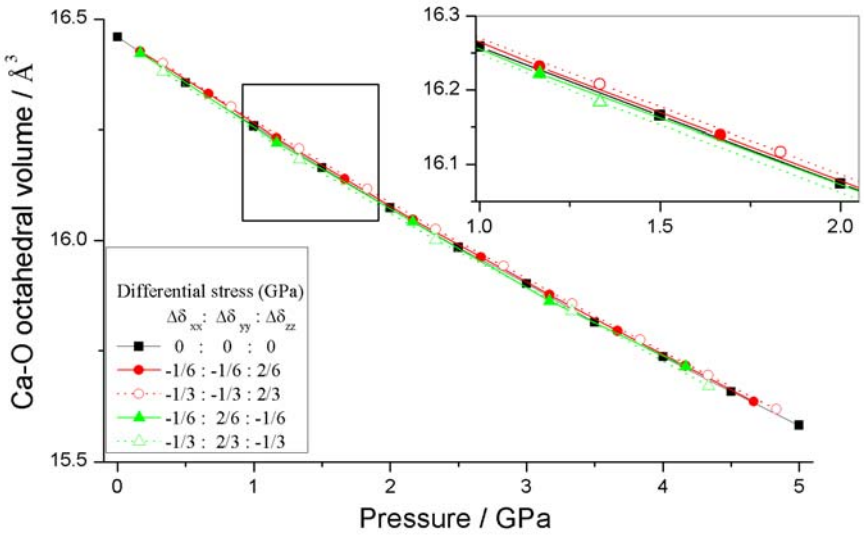

Fig.3. Changes of bond length and polyhedral volume of calcite with pressure.

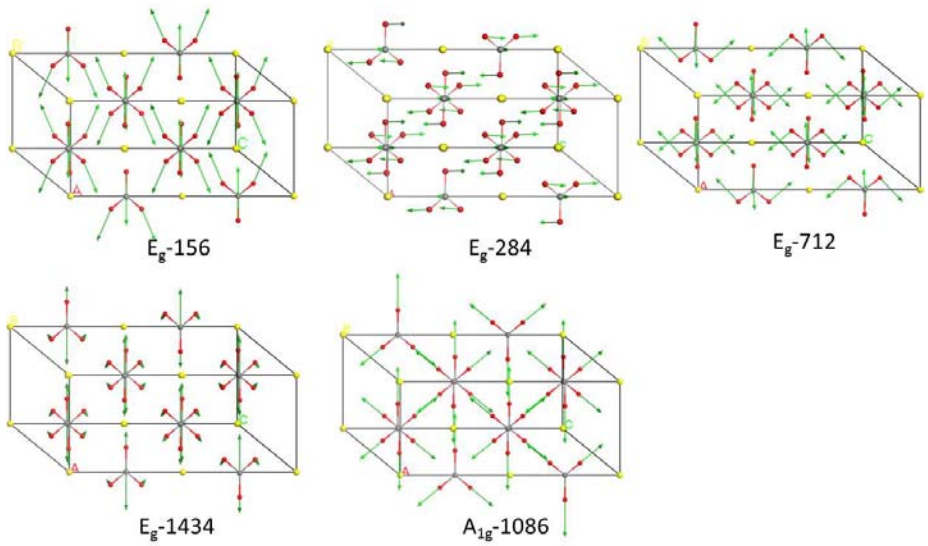

Fig. 4 Schematics of vibrational pattern of each calcite Raman mode (viewed from [101]). The arrows and their lengths indicate the direction of atomic motions and the relative vibrational intensities of atoms, respectively.

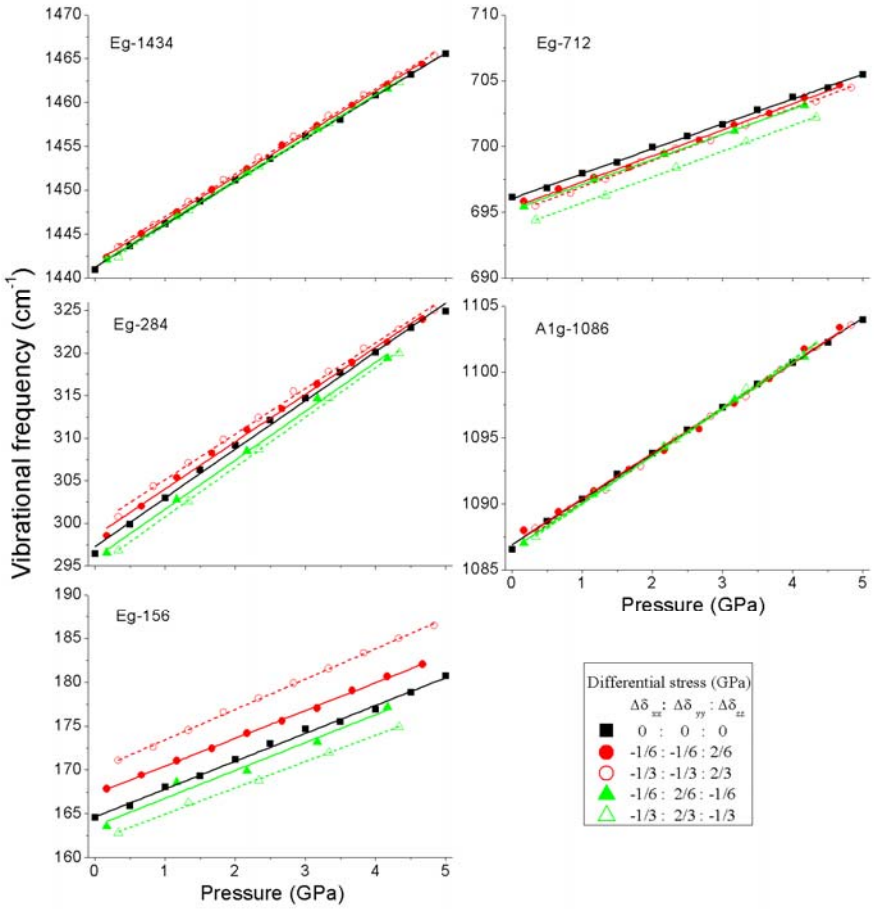

Fig. 5 Pressure dependence of the Raman vibrational frequencies of calcite

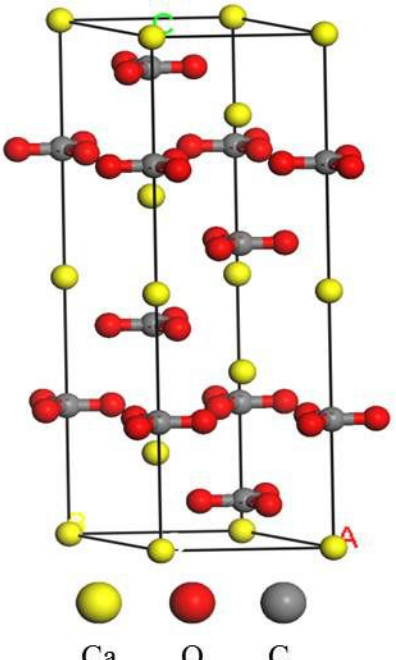

1

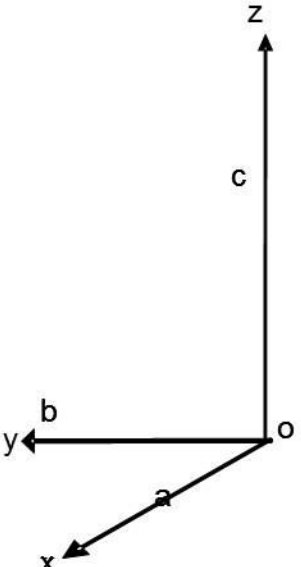

2

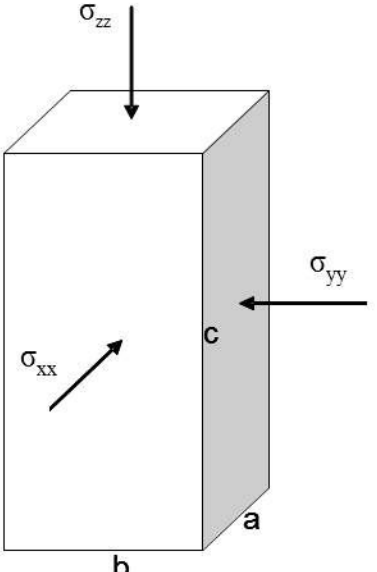

3

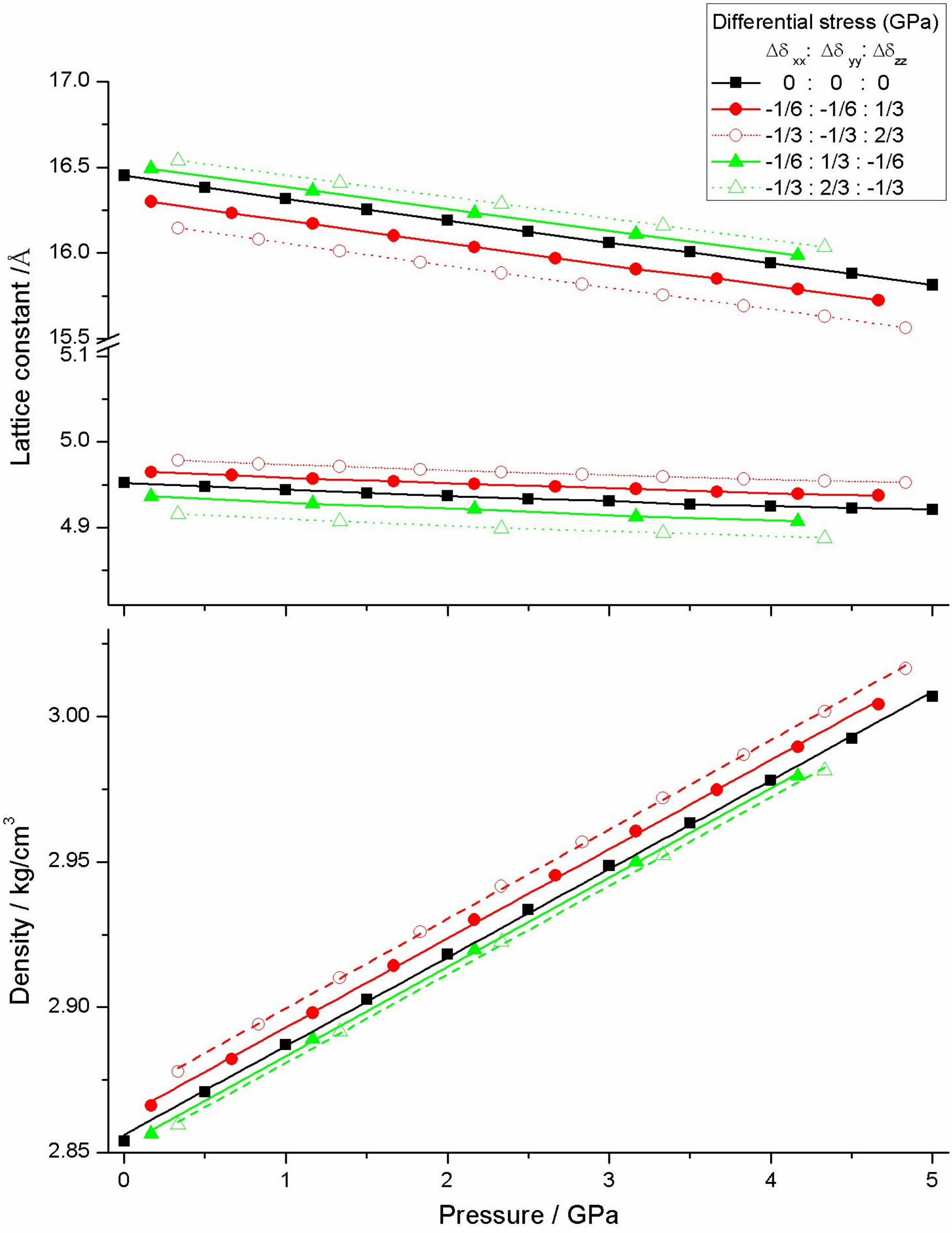
Differential stress (GPa)
Δδ xx: Δδ yy: Δδ zz
0 : 0 : 0
-1/6 : -1/6 : 1/3
-1/3 : -1/3 : 2/3
-1/6 : 1/3 : -1/6
-1/3 : 2/3 : -1/3
Lattice constant /Å
17.0
16.5
16.0
15.5
5.1
5.0
4.9
Density / kg/cm3
3.00
2.95
2.90
2.85
0
1
2
3
4
5
Pressure / GPa

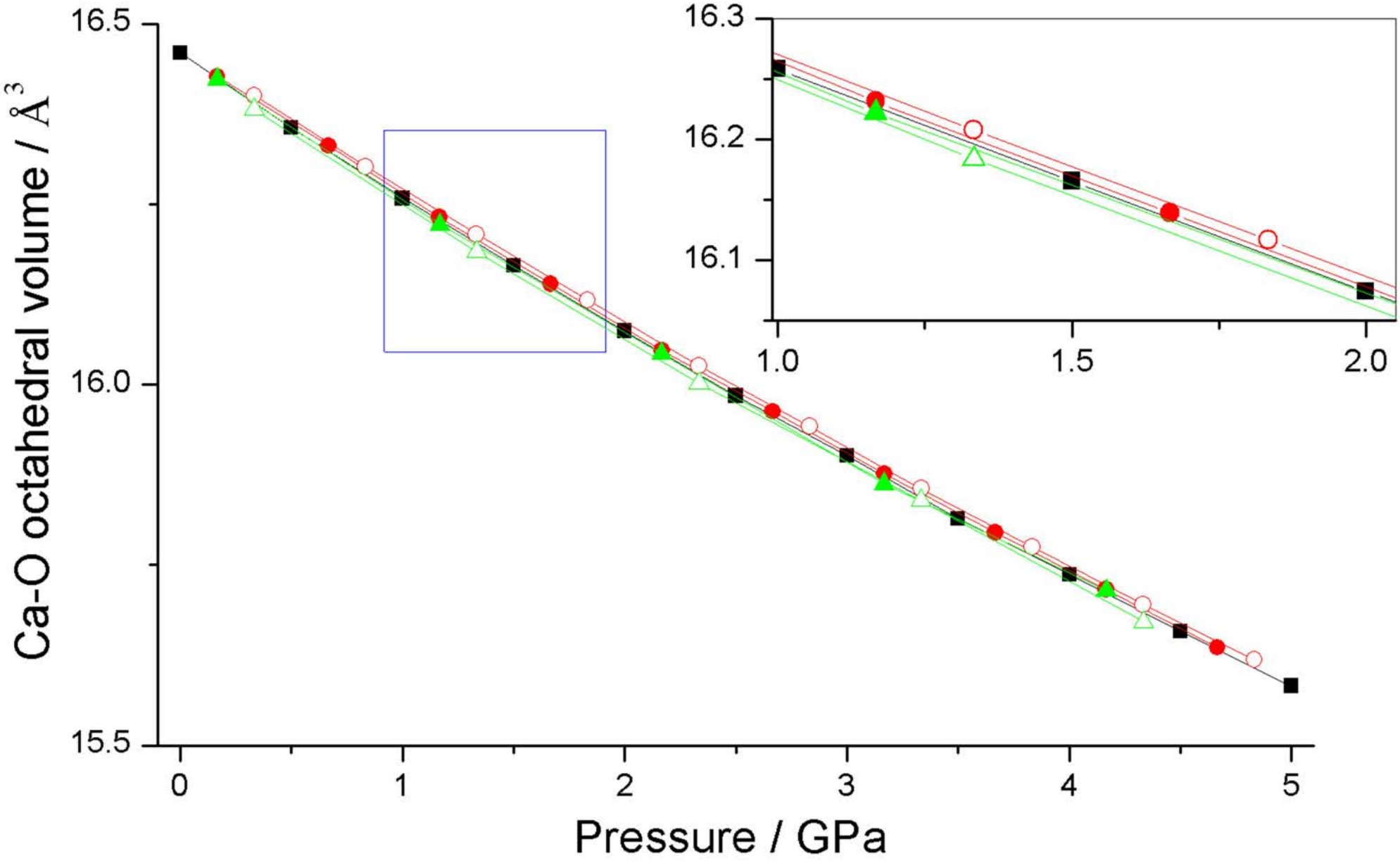
Ca-O octahedral volume / Å^3
16.5
16.0
15.5
0
1
2
3
4
5
Pressure / GPa
16.3
16.2
16.1
1.0
1.5
2.0

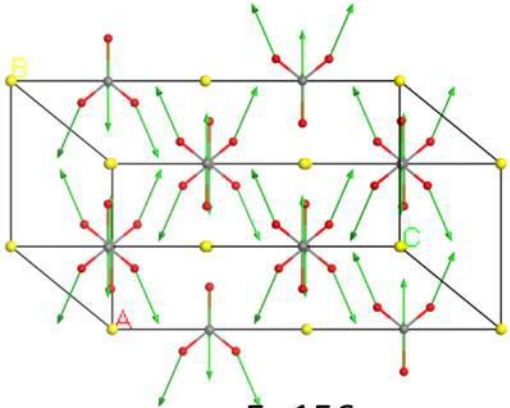

E_g-156

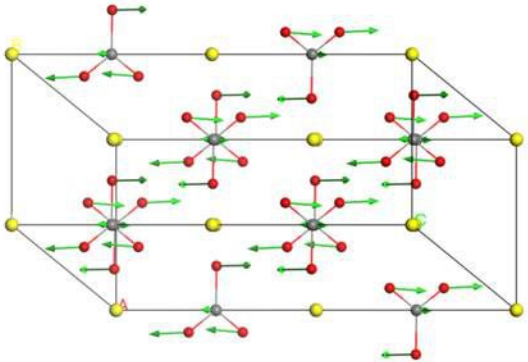

E_g-284

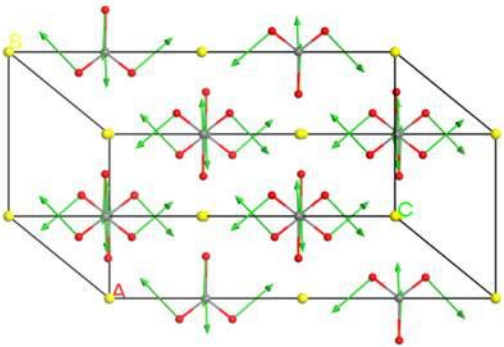

E_g-712

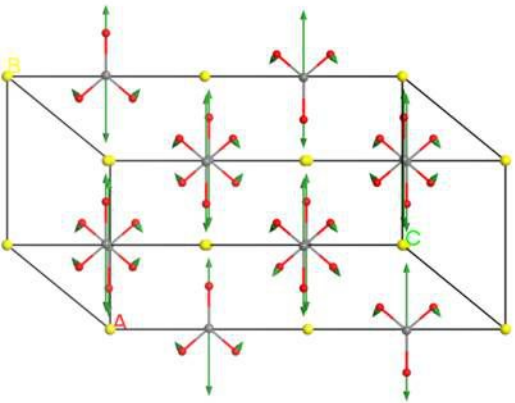

E_g-1434

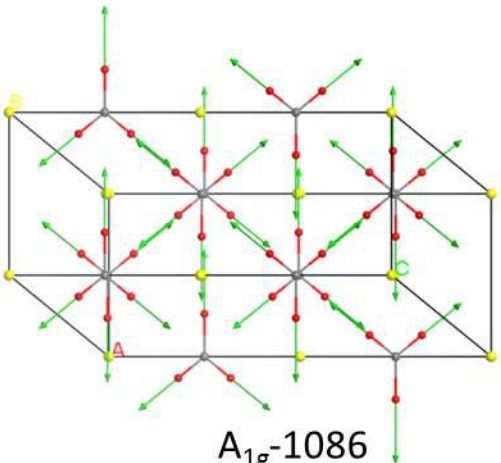

A_{1g}-1086

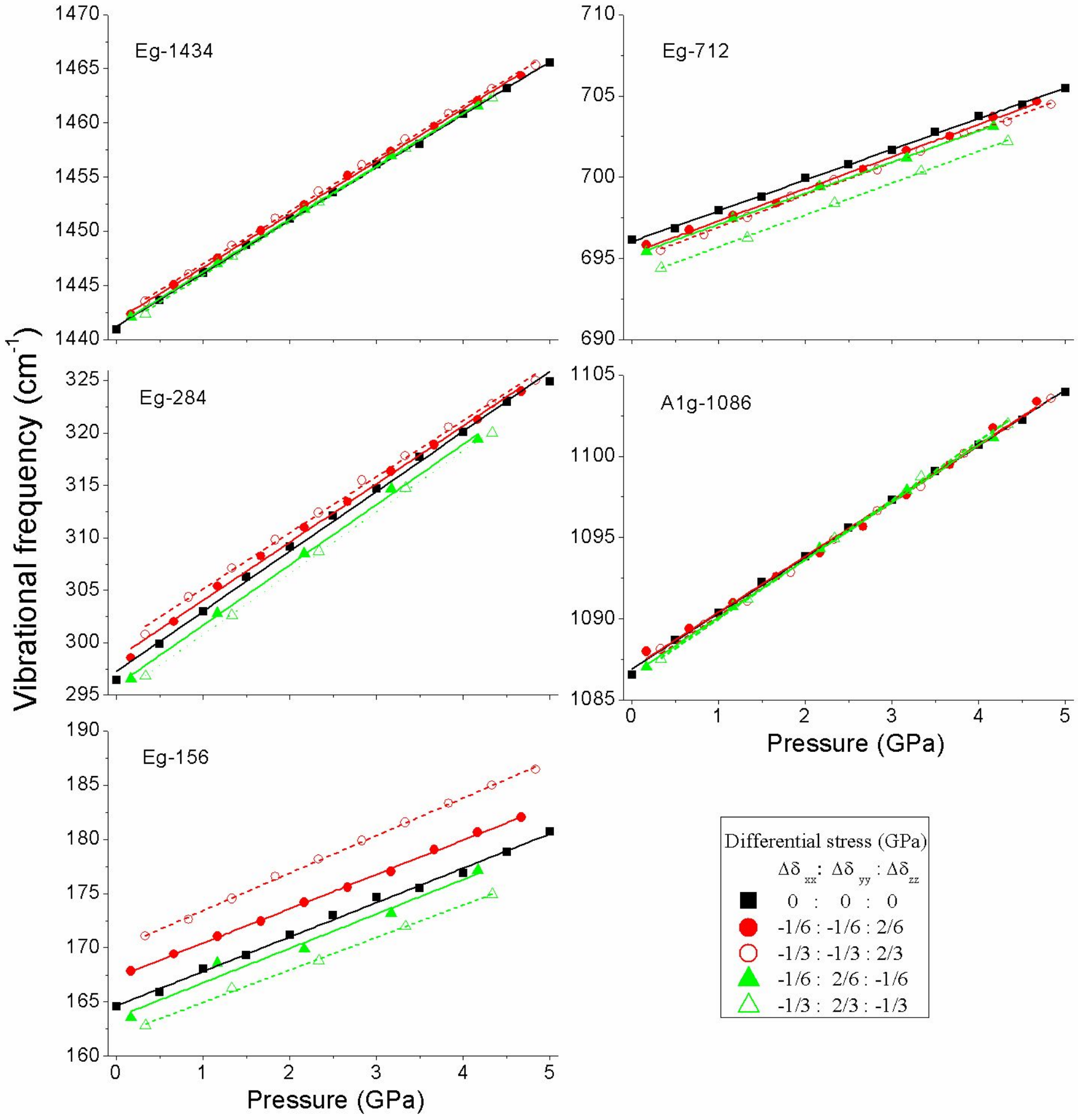
Eg-1434
Eg-712
Eg-284
A1g-1086
Eg-156
Vibrational frequency (cm-1)
Pressure (GPa)
Differential stress (GPa)
Δδxx : Δδyy : Δδzz
0 : 0 : 0
-1/6 : -1/6 : 2/6
-1/3 : -1/3 : 2/3
-1/6 : 2/6 : -1/6
-1/3 : 2/3 : -1/3